Hydrol. Earth Syst. Sci. Discuss., https://doi.org/10.5194/hess-2017-253
Manuscript under review for journal Hydrol. Earth Syst. Sci.
Discussion started: 15 June 2017
© Author(s) 2017. CC BY 3.0 License.

Hydrology and Earth System Sciences
Discussions

# Global change in flood and drought intensities under climate change in the 21st century

**Behzad Asadieh*, Nir Y. Krakauer**

Civil Engineering Department and NOAA-CREST, The City College of New York, City University of New York, New York, USA; basadie00@citymail.cuny.edu; nkrakauer@ccny.cuny.edu

* Correspondence to Behzad Asadieh: basadie00@citymail.cuny.edu

## Abstract

Global warming is expected to intensify the Earth's hydrological cycle and increase flood and drought risks. Changes in global high and low streamflow extremes over the 21st century under two warming scenarios are analyzed as indicators of hydrologic flood and drought intensity, using an ensemble of bias-corrected global climate model (GCM) fields fed into different global hydrological models (GHMs). Based on multi-model mean, approximately 37% and 43% of global land areas are exposed to increases in flood and drought intensities, respectively, by the end of the 21st century under RCP8.5 scenario. The average rates of increase in flood and drought intensities in those areas are projected to be 24.5% and 51.5%, respectively. Nearly 10% of the global land areas are under the potential risk of simultaneous increase in both flood and drought intensities, with average rates of 10.1 and 19.8%, respectively; further, these regions tend to be highly populated parts of the globe, currently holding around 30% of the world's population (over 2.1 billion people). In a world more than 4 degrees warmer by the end of the 21st century compared to the pre-industrial era (RCP8.5 scenario), increases in flood and drought intensities are projected to be nearly twice as large as in a 2 degree warmer world (RCP2.6 scenario). Results also show that GHMs contribute to more uncertainties in streamflow changes than the GCMs. Under both forcing scenarios, there is high model agreement for significant increases in streamflow of the regions near and above the Arctic Circle, and consequent increases in the freshwater inflow to the Arctic Ocean, while subtropical arid areas experience reduction in streamflow.

Hydrol. Earth Syst. Sci. Discuss., https://doi.org/10.5194/hess-2017-253
Manuscript under review for journal Hydrol. Earth Syst. Sci.
Discussion started: 15 June 2017
© Author(s) 2017. CC BY 3.0 License.

Hydrology and Earth System Sciences
Discussions

## 1. Introduction

Floods and droughts, the natural disasters with the highest cost in human lives (Dilley, 2005; IFRC, 2002), are projected to be intensified under anthropogenic global warming and climate change (Dai, 2011; Dankers et al., 2013; Field, 2012; Stocker et al., 2013). Observational records as well as global climate model (GCM) simulations both show that the amount of water vapor in the atmosphere increases at a rate of approximately 7% per K of increase in global mean temperature (Allen and Ingram, 2002; Held and Soden, 2006; Wentz et al., 2007), similar to dictation of the Clausius-Clapeyron equation conditional to stable relative humidity (Held and Soden, 2006; Pall et al., 2006). Increased amount of atmospheric water content is expected to intensify precipitation extremes (Allan and Soden, 2008; O'Gorman and Schneider, 2009; Trenberth, 2011), as evidenced by both observations and GCM simulations (Alexander et al., 2006; Asadieh and Krakauer, 2015, 2016; Kharin et al., 2013; Min et al., 2011; O'Gorman and Schneider, 2009; Stocker et al., 2013; Toreti et al., 2013; Westra et al., 2013), with relatively stronger impact than for mean precipitation (Asadieh and Krakauer, 2016; Lambert et al., 2008; Pall et al., 2006). Change in intensity and distribution of precipitation events under climate change is expected to increase the intensity and frequency of flood and drought events in many regions (Asadieh and Krakauer, 2015, 2016; Dankers et al., 2013; Field, 2012; Held and Soden, 2006; Min et al., 2011; O'Gorman and Schneider, 2009; Stocker et al., 2013).

Runoff projections from 3 GCMs show strong positive trend around high latitudes and negative trend for some mid-latitude regions, by the end of the 21$^{st}$ century (Hagemann et al., 2013). Another study of runoff projections from a larger ensemble of GCMs also confirms such trends in runoff for the 21$^{st}$ century (Tang and Lettenmaier., 2012). Changes in runoff, and consequently in streamflow, under current and future climate change has strong implications for available freshwater resources (Arnell, 2004; Brekke et al., 2009; Oki and Kanae, 2006; Stocker et al., 2013; Vörösmarty et al., 2000). Climate change is projected to decrease runoff in land areas around Mediterranean and some parts of Europe, southern Africa and central and southern America, and consequently increase water stress in those regions (Arnell, 2004). It is also projected to increase aridity in southern Europe and the Middle East, Australia, Southeast Asia, and large parts of Americas and Africa, in the 21st century (Dai, 2011).

Climate-change-induced decrease in mean precipitation and consequently runoff can increase water stress in such regions. Regions experiencing increase in total annual precipitation and runoff under climate change may also face increased water stress, as a result of change in precipitation and runoff distribution (Arnell, 2004; Asadieh and Krakauer, 2016;

Hydrol. Earth Syst. Sci. Discuss., https://doi.org/10.5194/hess-2017-253
Manuscript under review for journal Hydrol. Earth Syst. Sci.
Discussion started: 15 June 2017
© Author(s) 2017. CC BY 3.0 License.



Oki and Kanae, 2006). Implications of anthropogenic climate change for flood events are widely noted in the literature; However, there are few multi-model analyses of future change in streamflow extremes at global scale (Arnell, 2004; Dankers et al., 2013; Hirabayashi et al., 2008, 2013; Koirala et al., 2014; Schewe et al., 2013), or detection of regions that may experience simultaneous increases in both flood and drought intensities. A study of streamflow provided by the Inter-Sectoral Impact Model Intercomparison Project (ISI-MIP) (Warszawski et al., 2013) projects increases for the high latitudes, eastern Africa and India, and decreases in streamflow of Mediterranean and southern Europe as well as South America and southern parts of North America, by the end of the 21st century (Schewe et al., 2013), similar to some other studies (Hagemann et al., 2013; Tang and Lettenmaier., 2012). Another study of ISI-MIP streamflow projects increases in 30 year return period of high flow in major parts of Siberia and some regions around Southeast Asia, and decreases in northern and eastern Europe and some regions around western United States, by the end of the 21st century (Dankers et al., 2013). Approximately two-thirds of global land area are projected to experience positive trend in the magnitude and frequency of 30 year return period of high flow (Dankers et al., 2013), magnitude of 95th percentile of streamflow (Koirala et al., 2014), and magnitude of annual-maximum daily streamflow (Asadieh et al., 2016).

Accurate simulation of weather fields such as precipitation, as well as simulation of the diverse hydrological processes that lead to streamflow generation, are major sources of uncertainty in streamflow trend simulation. Some earlier adoptions of climate model projections for flooding studies utilized single state-of-the-art global hydrological models (GHMs) for flow routing and streamflow simulation under the GCM-simulated climate (Hirabayashi et al., 2013; Koirala et al., 2014). However, GHMs are also a major source of uncertainty, as flow routings in different GHMs using the same weather fields can result in markedly different flood and drought trend predictions (Giuntoli et al., 2015; Haddeland et al., 2011; Hagemann et al., 2013). Additionally, historical simulations of weather variables from GCMs have shown discrepancies compared to the observations (biases) (Asadieh and Krakauer, 2015; Ehret et al., 2012; Hempel et al., 2013; Krakauer and Fekete, 2014), which may affect the climate change impact projections using the GCM outputs (Hagemann et al., 2011, 2013). This issue is often solved utilizing bias correction methods, in which the mean value of the time series is adjusted according to the observational records, while supposedly preserving the trends (Hempel et al., 2013).

Hydrol. Earth Syst. Sci. Discuss., https://doi.org/10.5194/hess-2017-253
Manuscript under review for journal Hydrol. Earth Syst. Sci.
Discussion started: 15 June 2017
© Author(s) 2017. CC BY 3.0 License.



A study of change in 100-yr flood return period in the last 3 decades of the 21st century compared to the last 3 decades of the 20th century, projected by 11 GCMs under various emission scenarios, shows increased flood frequency over the South and Southeast Asia, northern Eurasia, South America, and tropical Africa (Hirabayashi et al., 2013). Another similar study investigates changes in 5th and 95th percentiles of flow, projected by the same 11 GCMs (Koirala et al., 2014). However, both these studies use a single state-of-the-art river routing model developed by the authors for streamflow data generation using the GCM inputs. A study of changes in frequency of 95th and 10th percentiles of streamflow in the 21st century, using multiple GCMs and GHMs from ISI-MIP, shows that the number of days with flow above the historical 95th percentile will significantly increases in the high latitudes and the number of days with flow below the historical 10th percentile will increases significantly in Mediterranean, southern North America, and Southern Hemisphere (Giuntoli et al., 2015). However, this study investigates changes in frequency of streamflow extremes, and not intensity.

Here, we use daily streamflow simulations from 25 GCM-GHM combinations (5 bias-corrected GCMs and 5 GHMs) from the ISI-MIP. We analyze simulated streamflow at the end of the 21st century (2070-2099, 21C) in comparison with the end of the 20th century (1971-2000, 20C). We study changes in the magnitude of the 95th percentile of annual streamflow (P95) in 21C compared to 20C, in which an increase would be an indication of increase in the flood intensity. We also study the change in the magnitude of the 5th percentile (P5), in which a decrease would correspond to an increase in the drought intensity. GHM-generated streamflow based on GCM inputs do not well capture the annual trends in flow compared to observations, even where, as in ISI-MIP, the GCM outputs are bias-corrected. However, the multi-decade average of bias-corrected ISI-MIP streamflow is shown to be more similar to that of observation-based streamflow simulations (Asadieh et al., 2016). Other studies have also used relative changes in multi-decade average of streamflow indices in a future 21C time window compared to a historical 20C time window for flooding and streamflow extremes analyses (Dankers et al., 2013; Hirabayashi et al., 2013; Koirala et al., 2014; Tang and Lettenmaier., 2012). Alongside the study of the magnitude of change, we also study the percentage of global population affected by changes in flood and/or drought intensities. Limiting global warming to 2 degrees Celsius above the pre-industrial era (achievable in RCP2.6 scenario (Moss et al., 2010; Stocker et al., 2013)) has been targeted in many scientific and governmental plans, for instance the 2015 Paris Climate Agreement

Hydrol. Earth Syst. Sci. Discuss., https://doi.org/10.5194/hess-2017-253
Manuscript under review for journal Hydrol. Earth Syst. Sci.
Discussion started: 15 June 2017
© Author(s) 2017. CC BY 3.0 License.



(UNFCCC, 2015). However, the increasing trajectory of emissions observed over the beginning on the 21st century, if continued, is more consistent with around 4 degrees Celsius of warming by the end of the century (similar to RCP 8.5 scenario (Moss et al., 2010; Stocker et al., 2013)). Hence, we study both low and high radiative forcing scenarios (RCP2.6 and RCP8.5) to investigate the impacts of 21C anthropogenic forcing on flood and drought risks.

## 2. Materials and Methods

We use daily streamflow data obtained from the first phase of the ISI-MIP (Warszawski et al., 2013). The ISI-MIP streamflow projections are produced by multiple GHMs, based on bias-corrected meteorological outputs of 5 GCMs from the fifth version of the Coupled Model Intercomparison Project (CMIP5) (Dankers et al., 2013), which are downscaled to 0.5 degree resolution for the period 1971-2099. The GCMs contributing to the first phase of ISI-MIP are: GFDL-ESM2M, HadGEM2-ES, IPSL-CM5A-LR, MIROC-ESM-CHEM and NorESM1-M (Warszawski et al., 2013). The 5 GHMs selected for this study are WBM, MacPDM, PCR-GLOBWB, DBH and LPJmL (refer to supplementary materials for details). ISI-MIP provides the streamflow outputs for only 5 GCMs, from more than 5 GHMs. Here, the number of GHMs is also limited to 5 so that the uncertainties arising from the GCMs and GHMs are readily comparable.

Relative changes in streamflow can be very large for individual grid cells, particularly in currently-frozen high latitudes. This bias averages across models and grid cells toward a positive trend, as the decreases are limited to 100% loss of the historic flow, while the increase can be well over 100% of the historic flow. Accordingly, changes are here normalized to between -1 and +1, so the ranges of increases and decreases are comparable. Normalized increase in the magnitude of P95 indicates increase in flood intensity, and is called the flood indicator. Since increased drought intensity corresponds to decrease in the magnitude of P5, the normalized changes in P5 are multiplied by -1 to form the drought indicator. We refer to positive/negative change in flood (drought) indicator as increased/decreased flood (drought) intensities, respectively.

Increase and decrease in flood and drought can form four combinations, which are categorized as the following four quadrants: 1. Increased flood and drought, 2. Increased flood and decreased drought, 3. Increased drought and decreased flood, and 4. Decreased flood and drought. Results obtained are averaged for each of these quadrants and the comparison of

Hydrol. Earth Syst. Sci. Discuss., https://doi.org/10.5194/hess-2017-253
Manuscript under review for journal Hydrol. Earth Syst. Sci.
Discussion started: 15 June 2017
© Author(s) 2017. CC BY 3.0 License.



results between different scenarios is made for each quadrant individually. Assignment of each grid cell to the specified quadrant is based on the averaged change across GCMs and GHMs.

In order to calculate the normalized change in flood intensity of a grid cell, the magnitude of the 95$^{th}$ percentile of daily streamflow (P95) is calculated for each year, and then averaged for 20C (called $Q_{20C}$) and 21C (called $Q_{21C}$). The normalized change is calculated as:

$$\Delta Q = \frac{Q_{21C} - Q_{20C}}{Q_{21C} + Q_{20C}} \quad \text{Eq.1}$$

The $\Delta Q$ value ranges between -1 and +1, where a normalized change equal to -1 indicates total loss of the 20C flow in the 21C and a normalized change equal to +1 indicates that all of the 21C flow is resultant of the change and the flow in 20C was zero. For normalized change in drought intensity of a grid cell, the same calculations are performed on the magnitude of the 5$^{th}$ percentile of annual streamflow (P5) and the $\Delta Q$ is multiplied by -1, so a positive number would indicate increase in hydrological drought intensity (decrease in low flow). Multi-model ensemble averages of changes are calculated based on the normalized change values. However, averaged normalized changes are then reverted to relative changes, and results are shown in both normalized change and relative percentages (cf. Figure S1).

We exclude the grid cells that have average daily flow below 0.01 mm over the period of 1971-200 (Hirabayashi et al., 2013). Greenland ice sheets are also excluded from the analysis. Grid cells remained to be studied, cover 75.9% of global land area, but include 95.9% of global population as of the year 2015. The grid cells with very low streamflow volume are excluded from the calculations, because such regions are very sensitive to changes projected by models and small increases in streamflow result in large relative changes in flood index, which may not meaningfully correspond to flooding risk for such dry regions. To identify the dry grid cells, the streamflow simulation of the WBM-plus model driven by reanalysis climate fields of WATCH Forcing Data (WFD) is used (Asadieh et al., 2016), as the ISI-MIP uses the WFD dataset for bias-correction of the GCM output (Hempel et al., 2013).

Calculation of normalized change in streamflow in 21C compared to 20C is performed on each of the 25 GCM-GHM combination datasets individually. The results are averaged over the models for each grid cell. The multi-model averages are then averaged over the grid cells that show increase in the indicator and also the over the grid cells that show decrease in the indicator (two separate values for each indicator). The multi-model averages are also averaged for each quadrant. This averaging gives a better sense of the projected magnitudes of flood and

© Author(s) 2017. CC BY 3.0 License.



drought intensity changes for each warming scenario in affected regions than averaging over all land areas, because the positive and negative trends cancel each other out in a global averaging due to the semi-symmetric behavior of changes (Figures 2.c and d). In a supplementary analysis, the streamflow data of all the model combinations were averaged first and the normalized change was calculated on the multimodel-averaged streamflow data. Both approaches yielded very similar results, indicating that the analyses are not sensitive to the method of averaging.

The two-sample t-test (Snedecor and Cochran, 1989) is used in this study to quantify the statistical significance level of difference between the means of the 20C and 21C streamflow time series (refer to supplementary materials). The percentage of land area with statistically significant change (at 95% confidence level) is reported. The affected population is calculated using the Gridded Population of the World (GPW) data from the Center for International Earth Science Information Network (CIESIN) (Doxsey-Whitfield et al., 2015).

## 3. Results and Discussion

Based on multi-model mean results under RCP8.5 scenario, 36.7% of global land area shows an increase in flood indicator (whose magnitude averages 24.55%), and 39.2% of land area shows an average of 21.10% decrease. On the other hand, 43.2% of global land area shows an average 51.40% increase in drought indicator, and 32.7% of land area shows 30.30% decrease (Table 1). Figure 1 shows global maps of normalized change in median, P5, and P95 of streamflow in 21C compared to 20C under two different warming scenarios, obtained from the ensemble mean of all 25 GCM-GHM combination datasets. Under RCP8.5 scenario, the high latitudes show an increase in all percentiles of flow, while the Mediterranean shores, Middle East, southern North America and the Southern Hemisphere show a decrease in all percentiles. The United Kingdom, some parts of Indonesia, India and southern Asia show an increase in the magnitude of P95 while experiencing a decrease in the magnitude of P5. Median flow shows a general pattern of change similar to P5. As shown in the figure, changes are more intense in RCP8.5 scenario (representative of 4 degrees warmer world in 21C compared to pre-industrial era) than in RCP2.6 scenario (representative of 2 degrees warmer world in 21C compared to pre-industrial era). However, unlike the RCP8.5 scenario, the RCP2.6 scenario projects increase in P95 for eastern United States as well as southern and western Europe. Global maps of change in median, P5, and P95 of streamflow for each individual model, are shown in supplemental Figures S2-7.

Hydrol. Earth Syst. Sci. Discuss., https://doi.org/10.5194/hess-2017-253
Manuscript under review for journal Hydrol. Earth Syst. Sci.
Discussion started: 15 June 2017
© Author(s) 2017. CC BY 3.0 License.



Figure 2 depicts the multi-model mean changes in flood and drought indicators averaged by latitude, as well as the scatter of the grid cells over the defined quadrants, under each RCP scenario. Results show increased flood and decreased drought in high latitudes, especially in the regions near and above the Arctic Circle, in both warming scenarios. The changes are projected with high agreement among the models in both scenarios, with greater change in RCP8.5 compared to RCP2.6 (Figure 2). This indicates future increase in the flow volume of the Arctic rivers and increased freshwater inflow into the Arctic Ocean, continuing the trend observed over the last decades (Peterson et al., 2002; Rawlins et al., 2010), which can be attributed to the thaw of permafrost and increased precipitation in a warmer climate. Rivers play a critical role in the Arctic freshwater system (Carmack et al., 2016; Lique et al., 2016), as river runoff is the major component of freshwater flux into the Arctic Ocean (Carmack et al., 2016). Arctic rivers' inflow to the Arctic Ocean accounts for around 10% of global annual water flux into the oceans (Haine et al., 2015; Lique et al., 2016). The projected increase in meltwater flux the Arctic Ocean may contribute to sea level rise and changes in water salinity, temperature as well as circulation in the Arctic Ocean (Peterson et al., 2002; Rawlins et al., 2010). The Southern Hemisphere shows a general increasing trend in drought and decrease in flood, indicating a negative trend in flow volume. The Northern Hemisphere tropics however show a mixed trend, as flood and drought mean changes averaged over latitude show fluctuations (Figure 2).

Figures 3 and 4 depict multi-model changes in flood and drought indicators under different warming scenarios, averaged over different latitudinal windows. Figure 3 shows the results from streamflow routings of each GHM based on inputs from multiple GCM simulations, where the thick lines in the plots denote the mean of change in the indicator and the shades denote ±1 st. dev. For each single GHM (shown by distinct colors), the thick line in the plots show the average of GCMs and the shading denotes the standard deviation of GCMs. Hence, the shadings in this figure are representative of uncertainties arising from GCMs. In the meantime, different average values (thick lines) means that different GHMs have produced different streamflow routings and different change values in the indicators, even though the routings are based on inputs from the same ensemble of GCMs. Figure 4, on the other hand, shows streamflow routings of multiple GHMs based on inputs from each of the GCMs, where the thick lines in the plots denote the mean of change in the indicator and the shades denote ±1 st. dev. For each single GCM (shown by distinct colors), the shading denotes the standard deviation of GHMs and hence, is representative of uncertainties arising from GHMs. The

© Author(s) 2017. CC BY 3.0 License.



RCP8.5 scenario show higher normalized change values and larger uncertainties, compared to the RCP2.6 scenario. The uncertainties are proportionally greater for drought trend projection than for flooding (Figure 3 and 4).

The shadings in the Figure 4 (GHM uncertainty representative) is wider than in the Figure 3 (GCM uncertainty representative), which shows that the GHMs contribute to higher rate of uncertainties in flood and drought change projections than GCMs. As seen in Figure 3 (c-d), for instance, drought predictions of the DBH hydrological model for Northern Hemisphere are significantly different from other hydrological models, even though the streamflow routings are based on the same GCM inputs. Such inconsistency between DBH models and other models' results may not be detectable, if the results are averaged as they are in the Figure 4. Wide shadings in Northern Hemisphere drought trends in Figure 4 (c-d) shows high uncertainties among the GHMs for that region, while the Figure 3 (c-d) reveals the major cause of such uncertainties to be the DBH model.

Figure 5 illustrates the global maps of combined change in flood and drought indicators under each RCP scenarios, obtained from the multi-model mean results of all 25 GCM-GHM combination datasets. Grid cells falling in each of the defined quadrants are shown with different colors, saturation of which is representative of the intensity of changes. As shown in the Figure, northern high latitudes, especially north Eurasia, northern Canada and Alaska, as well as eastern Africa and parts of South and Southeast Asia and Eastern Oceania show increase in flood intensity in both scenarios, similar to findings of earlier studies (Dankers et al., 2013; Hirabayashi et al., 2013; Schewe et al., 2013). Central America, Southern Africa, Middle East, Southern Europe, Mediterranean and major parts of South America and Australia show increase in drought intensity in both scenarios, comparable to findings of earlier studies (Arnell, 2004; Dai, 2011; Hagemann et al., 2013; Schewe et al., 2013). The United Kingdom and the shores of the North Sea as well as large parts of Tibetan, South Asia and Western Oceania show increase in both flood and drought intensities. In these cases, while preserving the direction of change, the RCP8.5 scenario projects stronger change compared to the RCP2.6 scenario. Southern and Western Europe and southern parts of the United States show small-magnitude, mixed increases in flood and drought intensities in RCP2.6 scenario. However, projections under RCP8.5 scenario are for strong increase in drought in those regions. Some parts of eastern Russia and northern United States show reduction in both flood and drought intensities (Figure 5). Compared to RCP2.6, the RCP8.5 scenario shows more expansion in drought intensity and less expansion in flood intensity (Figure 5 and Table 2).

© Author(s) 2017. CC BY 3.0 License.



Under the low radiative forcing scenario (RCP2.6), 45.4% of global land area shows increase in flood intensity in the multi-model mean and 36.4% shows increase in drought, indicating more land area exposure to flood intensity than to drought. The high radiative forcing scenario (RCP8.5) projects increased flood intensity in 36.6% of global land area and increased drought in 43.2%. Unlike the RCP2.6 scenario, the RCP8.5 scenario projects more land area exposure to drought intensity than to flood. Moreover, flood and drought events are more intense in RCP8.5 compared to RCP2.6, as the relative change values for 21C are nearly double; for instance, comparing the relative increases in flood indicator in Quad.2 (30.2% vs. 15.1%), and relative increases in drought indicator in Quad.3 (62.2% vs. 28.1%) (Table 3). Under RCP8.5 scenario, change in flood and drought indicators in 54.0 and 64.9%, respectively, of the global land area is statistically significant. The significance fraction is lower for the RCP2.6 scenario (38.4 and 53.8% of global land area in flood and drought indicators, respectively). The significance percentage is calculated for the multimodel-averaged streamflow time series in 21C compared to 20C, and the percentages for each individual model may be different. Under RCP8.5 scenario (and similarly in RCP2.6), nearly 9.6% of global land areas show both increase in flood and drought intensities. Unfortunately, these regions are dominantly highly populated parts of the globe, the residence of around 29.6% of the world's current population, or more than 2.1 billion people (Table 2). The 2015 Paris Climate Agreement, adopted at the 21st meeting of the Conference of Parties (COP21), targets to limit the global temperature rise "well below" 2°C above the pre-industrial levels (UNFCCC, 2015). Even though seeming to be ambitious, such an agreement in intergovernmental level is a start to motivate the developed countries producing the majority of greenhouse gases to limit emissions and finance the climate-resilient development in lower income economies.

## 4. Conclusion

Global daily streamflow simulations of 25 GCM-GHM combination datasets are analyzed to study the implications of increased GHG emissions and consequent atmospheric temperature rise for global streamflow extremes. The projected changes in high and low streamflow percentiles in the 21C compared to the 20C were studied, under both low and high radiative forcing scenarios, to investigate the regions projected to face increases in flood and/or drought events' intensities, and study the number of people affected by such changes. Multiple GHMs and GCMs are used to account for uncertainties arising from the hydrological models and flow routing process on the flood and drought studies, additional to the weather field simulation

© Author(s) 2017. CC BY 3.0 License.



uncertainties. Results suggest that northern high latitudes, especially north Eurasia, northern Canada and Alaska, as well as Tibetan and Southern India will face strong increases in flood intensities over the 21st century, while the Mediterranean shores, Middle East, southern North America and the Southern Hemisphere are projected to see strong increases in drought intensities. The projected increase in meltwater flux from the pan-Arctic watershed into the Arctic Ocean may contribute to sea level rise, and changes in salinity, temperature and circulation in the Arctic Ocean. The United Kingdom and the shores of the North Sea as well as large parts of Tibetan, South Asia and Western Oceania show increase in both flood and drought intensities. Regions projected to experience simultaneous increases in both flood and drought event intensities as a result of change in streamflow distribution, are highly populated parts of the globe, even though covering a small fraction of global land area. Results show that GHMs contribute to more uncertainties in streamflow changes than the GCMs, where different GHMs have produced different streamflow routings and different change values in the indicators, even though the routings are based on inputs from the same ensemble of GCMs. A world 2°C warmer than the pre-industrial era will still face increases in flood and drought in most regions. However, the GCM and GHM ensemble projects that 4°C of warming will bring nearly twice as much increase in the intensity of those events.

## Author Contribution

B. Asadieh and N.Y. Krakauer conceived and designed the experiment. B. Asadieh carried out the analyses and wrote the initial manuscript. B. Asadieh and N.Y. Krakauer analyzed the results, wrote the manuscript, and made the conclusions.

## Acknowledgments

The authors gratefully acknowledge support from NOAA under grants NA11SEC4810004, NA12OAR4310084 and NA15OAR4310080, and from PSC-CUNY Award # 68346-00 46. All statements made are the views of the authors and not the opinions of the funding agency or the U.S. government.

## Conflict of interest

The authors declare that they have no conflict of interest.

## References

Alexander, L. V., Zhang, X., Peterson, T. C., Caesar, J., Gleason, B., Klein Tank, A. M. G., Haylock, M., Collins, D., Trewin, B., Rahimzadeh, F., Tagipour, A., Rupa Kumar, K., Revadekar, J., Griffiths, G., Vincent, L.,

© Author(s) 2017. CC BY 3.0 License.



Stephenson, D. B., Burn, J., Aguilar, E., Brunet, M., Taylor, M., New, M., Zhai, P., Rusticucci, M. and Vazquez-Aguirre, J. L.: Global observed changes in daily climate extremes of temperature and precipitation, J. Geophys. Res., 111(D5), D05109, doi:10.1029/2005JD006290, 2006.

Allan, R. P. and Soden, B. J.: Atmospheric warming and the amplification of precipitation extremes, Science (80-. )., 321(5895), 1481–484, doi:10.1126/science.1160787, 2008.

Allen, M. R. and Ingram, W. J.: Constraints on future changes in climate and the hydrologic cycle, Nature, 419(6903), 224–232, doi:10.1038/nature01092, 2002.

Arnell, N. W.: Climate change and global water resources: SRES emissions and socio-economic scenarios, Glob. Environ. Chang., 14(1), 31–52, doi:10.1016/j.gloenvcha.2003.10.006, 2004.

Asadieh, B. and Krakauer, N. Y.: Global trends in extreme precipitation: climate models versus observations, Hydrol. Earth Syst. Sci., 19(2), 877–891, doi:10.5194/hess-19-877-2015, 2015.

Asadieh, B. and Krakauer, N. Y.: Impacts of changes in precipitation amount and distribution on water resources studied using a model rainwater harvesting system, JAWRA J. Am. Water Resour. Assoc., 1–22, doi:10.1111/1752-1688.12472, 2016.

Asadieh, B., Krakauer, N. Y. and Fekete, B. M.: Historical trends in mean and extreme runoff and streamflow based on observations and climate models, Water, 8(5), 189, doi:10.3390/w8050189, 2016.

Brekke, L. D., Maurer, E. P., Anderson, J. D., Dettinger, M. D., Townsley, E. S., Harrison, A. and Pruitt, T.: Assessing reservoir operations risk under climate change, Water Resour. Res., 45(4), 1–16, doi:10.1029/2008WR006941, 2009.

Carmack, E. C., Yamamoto-Kawai, M., Haine, T. W. N., Bacon, S., Bluhm, B. A., Lique, C., Melling, H., Polyakov, I. V., Straneo, F., Timmermans, M. L. and Williams, W. J.: Freshwater and its role in the Arctic Marine System: Sources, disposition, storage, export, and physical and biogeochemical consequences in the Arctic and global oceans, J. Geophys. Res. G Biogeosciences, 121(3), 675–717, doi:10.1002/2015JG003140, 2016.

Dai, A.: Drought under global warming: A review, Wiley Interdiscip. Rev. Clim. Chang., 2(1), 45–65, doi:10.1002/wcc.81, 2011.

Dankers, R., Arnell, N. W., Clark, D. B., Falloon, P. D., Fekete, B. M., Gosling, S. N., Heinke, J., Kim, H., Masaki, Y., Satoh, Y., Stacke, T., Wada, Y. and Wisser, D.: First look at changes in flood hazard in the Inter-Sectoral Impact Model Intercomparison Project ensemble, Proc. Natl. Acad. Sci., 111(9), 3257–3261, doi:10.1073/pnas.1302078110, 2013.

Dilley, M.: Natural disaster hotspots: a global risk analysis (Vol. 5), World Bank Publications., 2005.

Doxsey-Whitfield, E., MacManus, K., Adamo, S. B., Pistolesi, L., Squires, J., Borkovska, O. and Baptista, S. R.: Taking advantage of the improved availability of census data: a first look at the gridded population of the world, version 4 (GPWv4), Pap. Appl. Geogr., 1(3), 226–234, doi:10.1080/23754931.2015.1014272, 2015.

Ehret, U., Zehe, E., Wulfmeyer, V., Warrach-Sagi, K. and Liebert, J.: HESS Opinions "should we apply bias correction to global and regional climate model data?," Hydrol. Earth Syst. Sci., 16(9), 3391–3404, doi:10.5194/hess-16-3391-2012, 2012.

Field, C. B.: Managing the risks of extreme events and disasters to advance climate change adaptation: special report of the intergovernmental panel on climate change, Cambridge University Press, Cambridge, UK., 2012.

Giuntoli, I., Vidal, J. P., Prudhomme, C. and Hannah, D. M.: Future hydrological extremes: The uncertainty from multiple global climate and global hydrological models, Earth Syst. Dyn., 6(1), 267–285, doi:10.5194/esd-6-267-2015, 2015.

Haddeland, I., Clark, D. B., Franssen, W., Ludwig, F., Voß, F., Arnell, N. W., Bertrand, N., Best, M., Folwell, S., Gerten, D., Gomes, S., Gosling, S. N., Hagemann, S., Hanasaki, N., Harding, R., Heinke, J., Kabat, P., Koirala, S., Oki, T., Polcher, J., Stacke, T., Viterbo, P., Weedon, G. P. and Yeh, P.: Multimodel estimate of the global terrestrial water balance: setup and first results, J. Hydrometeorol., 12, 869–884, doi:10.1175/2011JHM1324.1, 2011.

Hagemann, S., Chen, C., Clark, D. B., Folwell, S., Gosling, S. N., Haddeland, I., Hanasaki, N., Heinke, J., Ludwig, F., Voss, F. and Wiltshire, A. J.: Climate change impact on available water resources obtained using multiple global climate and hydrology models, Earth Syst. Dyn., 4(1), 129–144, doi:10.5194/esd-4-129-2013, 2013.

© Author(s) 2017. CC BY 3.0 License.



Hagemann, S., Chen, C., Haerter, J. O., Heinke, J., Gerten, D. and Piani, C.: Impact of a statistical bias correction on the projected hydrological changes obtained from three GCMs and two hydrology models, J. Hydrometeorol., 12(4), 556–578, doi:10.1175/2011JHM1336.1, 2011.

Haine, T. W. N., Curry, B., Gerdes, R., Hansen, E., Karcher, M., Lee, C., Rudels, B., Spreen, G., de Steur, L., Stewart, K. D. and Woodgate, R.: Arctic freshwater export: Status, mechanisms, and prospects, Glob. Planet. Change, 125, 13–35, doi:10.1016/j.gloplacha.2014.11.013, 2015.

Held, I. M. and Soden, B. J.: Robust responses of the hydrological cycle to global warming, J. Clim., 19(21), 5686–5699, doi:10.1175/JCLI3990.1, 2006.

Hempel, S., Frieler, K., Warszawski, L., Schewe, J. and Piontek, F.: A trend-preserving bias correction – the ISI-MIP approach, Earth Syst. Dyn., 4(2), 219–236, doi:10.5194/esd-4-219-2013, 2013.

Hirabayashi, Y., Kanae, S., Emori, S., Oki, T. and Kimoto, M.: Global projections of changing risks of floods and droughts in a changing climate, Hydrol. Sci. J., 53(4), 754–772, doi:10.1623/hysj.53.4.754, 2008.

Hirabayashi, Y., Mahendran, R., Koirala, S., Konoshima, L., Yamazaki, D., Watanabe, S., Kim, H. and Kanae, S.: Global flood risk under climate change, Nat. Clim. Chang., 3(9), 816–821, doi:10.1038/nclimate1911, 2013.

IFRC: World disaster report, focus on reducing risk, edited by J. Walter, International Federation of Red Cross and Red Crescent Societies, Geneva, Switzerland. [online] Available from: https://www.ifrc.org/PageFiles/89755/2002/32600-WDR2002.pdf, 2002.

Kharin, V. V., Zwiers, F. W., Zhang, X. and Wehner, M.: Changes in temperature and precipitation extremes in the CMIP5 ensemble, Clim. Change, 119(2), 345–357, doi:10.1007/s10584-013-0705-8, 2013.

Koirala, S., Hirabayashi, Y., Mahendran, R. and Kanae, S.: Global assessment of agreement among streamflow projections using CMIP5 model outputs, Environ. Res. Lett., 9(6), 64017, doi:10.1088/1748-9326/9/6/064017, 2014.

Krakauer, N. Y. and Fekete, B. M.: Are climate model simulations useful for forecasting precipitation trends? Hindcast and synthetic-data experiments, Environ. Res. Lett., 9(2), 24009, doi:10.1088/1748-9326/9/2/024009, 2014.

Lambert, F. H., Stine, A. R., Krakauer, N. Y. and Chiang, J. C. H.: How much will precipitation increase with global warming?, Eos, Trans. Am. Geophys. Union, 89(21), 193–194, doi:10.1029/2008EO210001, 2008.

Lique, C., Holland, M. M., Dibike, Y. B., Lawrence, D. M. and Screen, J. A.: Modeling the Arctic freshwater system and its integration in the global system: Lessons learned and future challenges, J. Geophys. Res. G Biogeosciences, 121(3), 540–566, doi:10.1002/2015JG003120, 2016.

Min, S.-K., Zhang, X., Zwiers, F. W. and Hegerl, G. C.: Human contribution to more-intense precipitation extremes, Nature, 470(7334), 378–81, doi:10.1038/nature09763, 2011.

Moss, R. H., Edmonds, J. a, Hibbard, K. a, Manning, M. R., Rose, S. K., van Vuuren, D. P., Carter, T. R., Emori, S., Kainuma, M., Kram, T., Meehl, G. a, Mitchell, J. F. B., Nakicenovic, N., Riahi, K., Smith, S. J., Stouffer, R. J., Thomson, A. M., Weyant, J. P. and Wilbanks, T. J.: The next generation of scenarios for climate change research and assessment, Nature, 463(7282), 747–756, doi:10.1038/nature08823, 2010.

O'Gorman, P. A. and Schneider, T.: The physical basis for increases in precipitation extremes in simulations of 21st-century climate change, Proc. Natl. Acad. Sci., 106(16), 14773–14777, doi:10.1073/pnas.0907610106, 2009.

Oki, T. and Kanae, S.: Global hydrological cycles and world water resources, Science (80-. )., 313(5790), 1068–1072, doi:10.1126/science.1128845, 2006.

Pall, P., Allen, M. R. and Stone, D. A.: Testing the Clausius–Clapeyron constraint on changes in extreme precipitation under CO2 warming, Clim. Dyn., 28(4), 351–363, doi:10.1007/s00382-006-0180-2, 2006.

Peterson, B. J., Holmes, R. M., McClelland, J. W., Vörösmarty, C. J., Lammers, R. B., Shiklomanov, A. I., Shiklomanov, I. a and Rahmstorf, S.: Increasing river discharge to the Arctic Ocean, Science (80-. )., 298(5601), 2171–2173, doi:10.1126/science.1077445, 2002.

Rawlins, M. A., Steele, M., Holland, M. M., Adam, J. C., Cherry, J. E., Francis, J. A., Groisman, P. Y., Hinzman, L. D., Huntington, T. G., Kane, D. L., Kimball, J. S., Kwok, R., Lammers, R. B., Lee, C. M., Lettenmaier, D. P., Mcdonald, K. C., Podest, E., Pundsack, J. W., Rudels, B., Serreze, M. C., Shiklomanov, A., Skagseth, O., Troy, T. J., Vorosmarty, C. J., Wensnahan, M., Wood, E. F., Woodgate, R., Yang, D., Zhang, K. and Zhang,

© Author(s) 2017. CC BY 3.0 License.



T.: Analysis of the Arctic system for freshwater cycle intensification: Observations and expectations, J. Clim., 23(21), 5715–5737, doi:10.1175/2010JCLI3421.1, 2010.

Schewe, J., Heinke, J., Gerten, D., Haddeland, I., Arnell, N. W., Clark, D. B., Dankers, R., Eisner, S., Fekete, B. M., Colón-González, F. J., Gosling, S. N., Kim, H., Liu, X., Masaki, Y., Portmann, F. T., Satoh, Y., Stacke, T., Tang, Q., Wada, Y., Wisser, D., Albrecht, T., Frieler, K., Piontek, F., Warszawski, L. and Kabat, P.: Multimodel assessment of water scarcity under climate change, Proc. Natl. Acad. Sci., 111(9), 3245–3250, doi:10.1073/pnas.1222460110, 2013.

Snedecor, G. W. and Cochran, W. G.: Statistical methods, 8thEdn, Iowa State University Press, Iowa., 1989.

Stocker, T. F., Qin, D., Plattner, G.-K., Tignor, M. M. B., Allen, S. K., Boschung, J., Nauels, A., Xia, Y., Bex, V. and Midgley, P. M.: Climate change 2013: The physical science basis. Working group I contribution to the fifth assessment report of the Intergovernmental Panel on Climate Change, Cambridge University Press., 2013.

Tang, Q. and Lettenmaier., D. P.: 21st century runoff sensitivities of major global river basins, Geophys. Res. Lett., 39(6), doi:10.1029/2011GL050834, 2012.

Toreti, A., Naveau, P., Zampieri, M., Schindler, A., Scoccimarro, E., Xoplaki, E., Dijkstra, H. A., Gualdi, S. and Luterbacher, J.: Projections of global changes in precipitation extremes from Coupled Model Intercomparison Project Phase 5 models, Geophys. Res. Lett., 40(18), 4887–4892, doi:10.1002/grl.50940, 2013.

Trenberth, K. E.: Changes in precipitation with climate change, Clim. Res., 47(1), 123–138, doi:10.3354/cr00953, 2011.

UNFCCC: Adoption of the Paris Agreement (FCCC/CP/2015/L.9/Rev.1). [online] Available from: http://unfccc.int/resource/docs/2015/cop21/eng/l09r01.pdf, 2015.

Vörösmarty, C. J., Green, P., Salisbury, J. and Lammers, R. B.: Global water resources: vulnerability from climate change and population growth, Science (80-. )., 289(5477), 284–288, doi:10.1126/science.289.5477.284, 2000.

Warszawski, L., Frieler, K., Huber, V., Piontek, F., Serdeczny, O. and Schewe, J.: The Inter-Sectoral Impact Model Intercomparison Project (ISI-MIP): Project framework, Proc. Natl. Acad. Sci., 111(9), 1–5, doi:10.1073/pnas.1312330110, 2013.

Wentz, F. J., Ricciardulli, L., Hilburn, K. and Mears, C.: How much more rain will global warming bring?, Science (80-. )., 317(5835), 233–235, doi:10.1126/science.1140746, 2007.

Westra, S., Alexander, L. V. and Zwiers, F. W.: Global increasing trends in annual maximum daily precipitation, J. Clim., 26(11), 3904–3918, doi:10.1175/JCLI-D-12-00502.1, 2013.

Hydrol. Earth Syst. Sci. Discuss., https://doi.org/10.5194/hess-2017-253
Manuscript under review for journal Hydrol. Earth Syst. Sci.
Discussion started: 15 June 2017
© Author(s) 2017. CC BY 3.0 License.

Hydrology and Earth System Sciences
Discussions
Open Access
EGU

Table 1. Multi-model average change in flood and drought indicators, as well as percent of population and land area affected by each category, for RCP2.6 and RCP8.5 scenarios. Presented percentages are for total global land area and total global population, and sum up to the 75.9% of global land area and 95.9% of the year 2015 total global population considered in this study. The value of change for indicators are normalized change and the numbers in parenthesis show the changes reverted to the relative percentages.

| | Percent of Change, in flood or drought | | Land Area Affected (% of total 148.9 million $km^2$, sum up to 75.9%) | | Population Affected (% of total 7.13 billion people, sum up to 95.9%) | |
|---|---|---|---|---|---|---|
| | RCP 8.5 | RCP 2.6 | RCP 8.5 | RCP 2.6 | RCP 8.5 | RCP 2.6 |
| Flood Increased Cells | 0.1093 (24.55 % rel.) | 0.0606 (12.90 % rel.) | 36.7% | 45.4% | 53.7% | 62.7% |
| Flood Decreased Cells | -0.1178 (-21.10 % rel.) | -0.0539 (-10.25 % rel.) | 39.2% | 30.5% | 42.2% | 32.2% |
| Drought Increased Cells | 0.2045 (51.40 % rel.) | 0.1029 (22.95 % rel.) | 43.2% | 36.3% | 67.8% | 56.1% |
| Drought Decreased Cells | -0.1784 (-30.30 % rel.) | -0.1018 (-18.50 % rel.) | 32.7% | 39.6% | 28.1% | 39.8% |

Hydrol. Earth Syst. Sci. Discuss., https://doi.org/10.5194/hess-2017-253
Manuscript under review for journal Hydrol. Earth Syst. Sci.
Discussion started: 15 June 2017
© Author(s) 2017. CC BY 3.0 License.

Hydrology and Earth System Sciences
Discussions

Table 2. Percent of population and land area affected by each flood and drought change quadrants, for RCP2.6 and RCP8.5 scenarios. Presented percentages are for total global land area and total global population. Hence, the percentages presented for quads. 1-4 sum up to the 75.9% of global land area and 95.9% of the year 2015 total global population considered in this study.

| | | Quad. 1. flood and drought increased | Quad. 2. flood increased, drought decreased | Quad. 3. drought increased, flood decreased | Quad. 4. flood and drought decreased |
|---|---|---|---|---|---|
| Land area affected (% of total 148.9 million km$^2$) | RCP8.5 | 9.6% | 27.0% | 33.6% | 5.7% |
| | RCP2.6 | 10.8% | 34.5% | 25.5% | 5.1% |
| Population affected (% of total 7.13 billion people) | RCP8.5 | 29.6% | 24.1% | 38.2% | 4.0% |
| | RCP2.6 | 27.1% | 35.6% | 28.9% | 4.3% |

Hydrol. Earth Syst. Sci. Discuss., https://doi.org/10.5194/hess-2017-253
Manuscript under review for journal Hydrol. Earth Syst. Sci.
Discussion started: 15 June 2017
© Author(s) 2017. CC BY 3.0 License.

Hydrology and Earth System Sciences
Open Access
Discussions

Table 3. Multi-model average change in flood and drought indicators, averaged for each quadrant, for RCP2.6 and RCP8.5 scenarios. The numbers show the normalized change and the numbers in parenthesis show the changes reverted to the relative percentages.

| | Quad. 1. flood and drought increased | | Quad. 2. flood increased, drought decreased | | Quad. 3. drought increased, flood decreased | | Quad. 4. flood and drought decreased | |
|---|---|---|---|---|---|---|---|---|
| | Change in flood | Change in drought | Change in flood | Change in drought | Change in flood | Change in drought | Change in flood | Change in drought |
| RCP8.5 | 0.0481 (10.10 %) | 0.0901 (19.80 %) | 0.1311 (30.20 %) | -0.1909 (-32.05 %) | -0.1290 (-22.85 %) | 0.2372 (62.20 %) | -0.0508 (-9.65 %) | -0.1183 (-21.15 %) |
| RCP2.6 | 0.0306 (6.30 %) | 0.0556 (11.80 %) | 0.0700 (15.05 %) | -0.1074 (-19.40 %) | -0.0593 (-11.20 %) | 0.1230 (28.05 %) | -0.0267 (-5.20 %) | -0.0635 (-11.95 %) |

Hydrol. Earth Syst. Sci. Discuss., https://doi.org/10.5194/hess-2017-253
Manuscript under review for journal Hydrol. Earth Syst. Sci.
Discussion started: 15 June 2017
© Author(s) 2017. CC BY 3.0 License.

Hydrology and Earth System Sciences
Discussions
Open Access
EGU

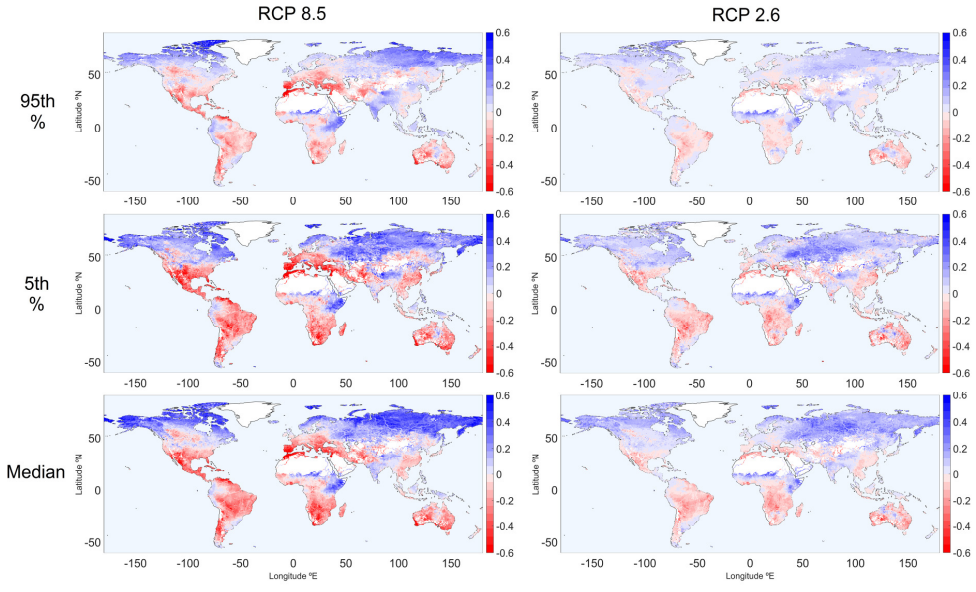


Figure 1. Global maps of normalized change in different streamflow percentiles (95th, 5th and median), under the RCP8.5 and RCP2.6 scenarios. Maps show the ensemble mean results of all 25 models. It should be noted that the results presented are the values of the change in different percentiles and are not necessarily equal to the defined flood and drought indicators.

Hydrol. Earth Syst. Sci. Discuss., https://doi.org/10.5194/hess-2017-253
Manuscript under review for journal Hydrol. Earth Syst. Sci.
Discussion started: 15 June 2017
© Author(s) 2017. CC BY 3.0 License.

Hydrology and Earth System Sciences
Discussions
Open Access
EGU

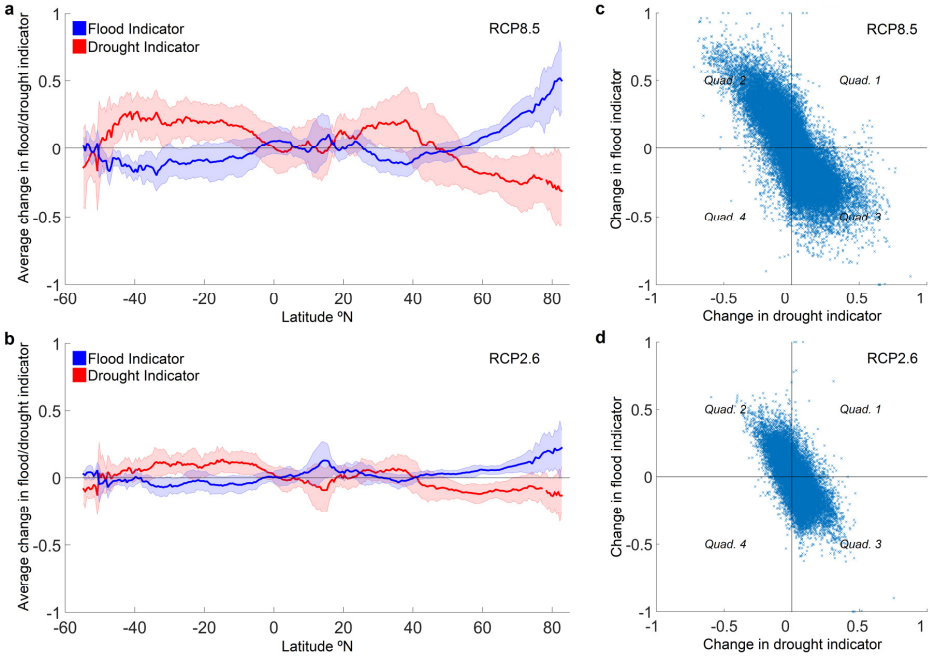


Figure 2. Multi-model change in flood and drought indicators under (a) RCP8.5 and (b) RCP2.6 scenarios, averaged by latitude, and scatter plot of change in flood and drought indicators for each grid cell under (c) RCP8.5 and (d) RCP2.6 scenarios. The thick line in the panels a and b show the ensemble mean value of all 25 GCM-GHM combination datasets and the shading denotes ±1 st. dev.

Hydrol. Earth Syst. Sci. Discuss., https://doi.org/10.5194/hess-2017-253
Manuscript under review for journal Hydrol. Earth Syst. Sci.
Discussion started: 15 June 2017
© Author(s) 2017. CC BY 3.0 License.

Hydrology and Earth System Sciences
Discussions
Open Access
EGU

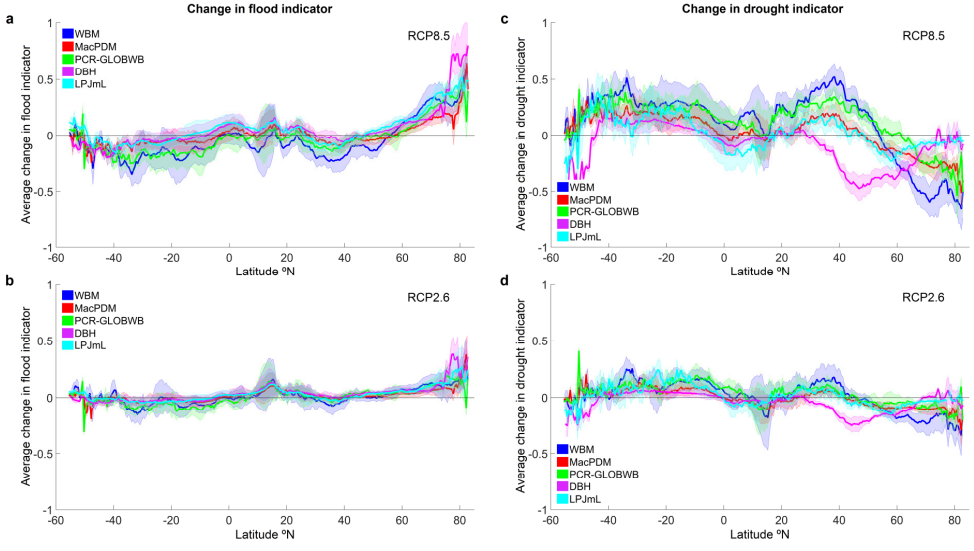


Figure 3. Multi-model change in flood indicator under RCP8.5 (a) and RCP2.6 (b) scenarios, and change in drought indicator under RCP8.5 (c) and RCP2.6 (d) scenarios, averaged by latitude. The thick lines in the plots show the mean change in the indicator, based on the streamflow routings of each GHM based on inputs from multiple GCMs, and the shades denote ±1 st. dev.

Hydrol. Earth Syst. Sci. Discuss., https://doi.org/10.5194/hess-2017-253
Manuscript under review for journal Hydrol. Earth Syst. Sci.
Discussion started: 15 June 2017
© Author(s) 2017. CC BY 3.0 License.

Hydrology and Earth System Sciences
Discussions
Open Access
EGU

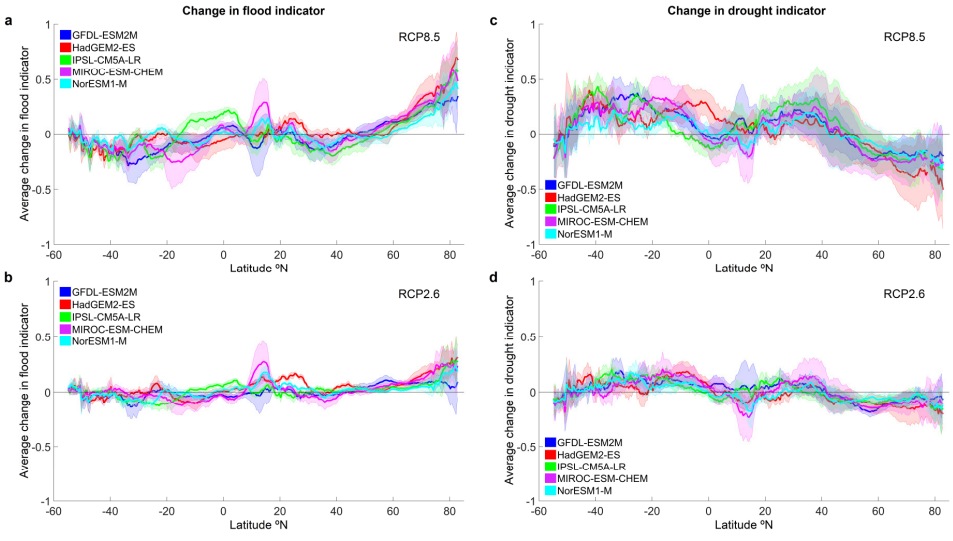


Figure 4. Multi-model change in flood indicator under RCP8.5 (a) and RCP2.6 scenarios (b), and change in drought indicator under RCP8.5 (c) and RCP2.6 scenarios (d), averaged by latitude. The thick lines in the plots show the mean change in the indicator, based on the streamflow from each GCM's simulated climate routed by multiple GHMs, and the shading denotes ±1 st. dev.

Hydrol. Earth Syst. Sci. Discuss., https://doi.org/10.5194/hess-2017-253
Manuscript under review for journal Hydrol. Earth Syst. Sci.
Discussion started: 15 June 2017
© Author(s) 2017. CC BY 3.0 License.

Hydrology and Earth System Sciences
Discussions
Open Access
EGU

1

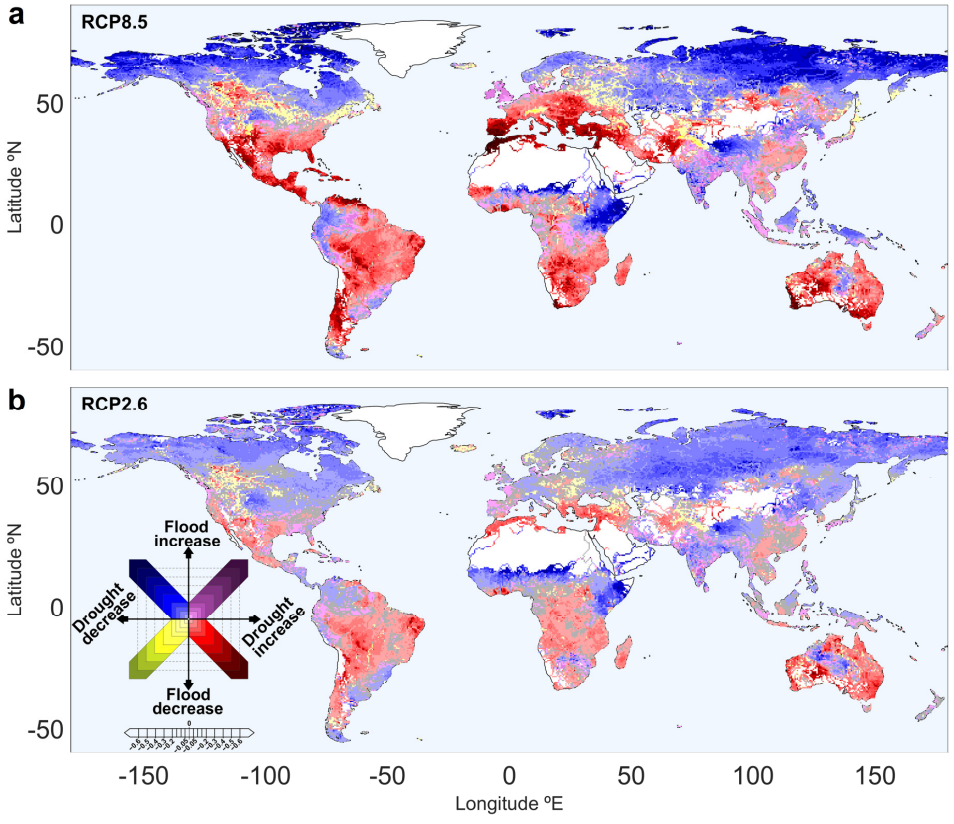


2

3 Figure 5. Global map of combined change in flood and drought indicators under (a)
4 RCP8.5 and (b) RCP2.6 scenario. The maps show the ensemble mean results of all 25
5 GCM-GHM combination datasets. Grid cells with increase in both flood and drought
6 (Quad. 1) are shown in purple shade, cells with increased flood (Quad. 2) and drought
7 (Quad. 3) are shown in blue and red shades, respectively, and cells with decrease in
8 both flood and drought (Quad. 4) are shown in yellow shade. The saturation of colors
9 shows the intensity of change, based on the normalized change in indicators, as shown
10 in the legend. Distribution of cells in each of the quadrants are comparable to the
11 Figures 2.c and d. Grid cells with normalized changes less than 1% (equal to 2% in
12 relative terms) in each quadrant are considered as no change cells and are shown in
13 gray. Grid cells excluded from the calculations are shown in white.